LETTER

https://doi.org/10.1038/s41586-018-0739-1

An experiment to search for dark-matter interactions using sodium iodide detectors

The COSINE-100 Collaboration*

Observations of galaxies and primordial radiation suggest that the Universe is made mostly of non-luminous dark matter[1,2]. Several new types of fundamental particle have been proposed as candidates for dark matter[3], such as weakly interacting massive particles (WIMPs)[4,5]. These particles would be expected to interact with nuclei in suitable detector materials on Earth, for example, causing them to recoil. However, no definitive signal from such dark-matter interactions has been detected despite concerted efforts by many collaborations[6]. One exception is the much-debated claim by the DAMA collaboration of a statistically significant (more than nine standard deviations) annual modulation in the rate of nuclear interaction events. Annual modulation is expected because of the variation in Earth's velocity relative to the Galaxy's dark-matter halo that arises from Earth's orbital motion around the Sun. DAMA observed a modulation in the rate of interaction events in their detector[7–9] with a period and phase consistent with that expected for WIMPs[10–12]. Several groups have been working to develop experiments with the aim of reproducing DAMA's results using the same target medium (sodium iodide)[13–17]. To determine whether there is evidence for an excess of events above the expected background in sodium iodide and to look for evidence of an annual modulation, the COSINE-100 experiment uses sodium iodide as the target medium to carry out a model-independent test of DAMA's claim. Here we report results from the initial operation of the COSINE-100 experiment related to the first task[18,19]. We observe no excess of signal-like events above the expected background in the first 59.5 days of data from COSINE-100. Assuming the so-called standard dark-matter halo model, this result rules out WIMP–nucleon interactions as the cause of the annual modulation observed by the DAMA collaboration[20–23]. The exclusion limit on the WIMP–sodium interaction cross-section is 1.14×10^{-40} cm^2 for 10-GeV c^{-2} WIMPs at a 90% confidence level. The COSINE-100 experiment will continue to collect data for two more years, enabling a model-independent test of the annual modulation observed by the DAMA collaboration.

COSINE-100 is located at the Yangyang Underground Laboratory in South Korea and began collecting data in 2016. The experiment uses eight thallium-doped sodium iodide crystals, arranged in a 4×2 array, with a total mass of 106 kg. The crystals were grown especially for the experiment to contain low levels of radioactive contaminants. Each crystal is coupled to two photomultiplier tubes (PMTs) to measure the amount of energy deposited in the crystal by a particle interaction. The sodium iodide crystal assemblies are immersed in 2,200 l of liquid scintillator, which enables the identification and subsequent reduction of radioactive backgrounds detected by the crystals[24]. The liquid scintillator is surrounded by copper, lead and plastic scintillator to reduce the background contribution from external radiation and cosmic-ray muons[25] (Extended Data Fig. 1).

The data used in this analysis were acquired between 20 October 2016 and 19 December 2016, with a total exposure of 59.5 live days. During this two-month period, no substantial environmental abnormalities or unstable detector performance were observed. The analysis was performed with all eight crystals. Six of the crystals have light yields of about 15 photoelectrons per kiloelectronvolt, with an analysis threshold of 2 keV. The other two crystals have lower light yields and require higher analysis thresholds (4 keV and 8 keV)[18]. Because the direct effect of these two crystals on the experiment is not substantial, here we discuss the spectra of only the six crystals with lower thresholds. When both PMTs on the same crystal register signals that are consistent with at least one photoelectron within 200 ns, that crystal is considered to have registered a 'hit'. The outputs of all of the detector elements during 8-μs time windows surrounding the hit time are recorded.

A nucleus recoiling from an interaction with a WIMP is expected to produce a hit in a single crystal. We select a set of candidate events by applying several criteria to reject backgrounds. We use boosted decision trees[26] (BDTs; a type of multivariate machine learning algorithm) to characterize the pulse shapes of the scintillation photons to discriminate PMT-induced noise events from radiation-induced events. Events that had hits in multiple crystals, the liquid scintillator or the muon detector are also rejected as multiple-hit events. Although multiple-hit events are not used for the WIMP search, they are used to develop the event selection criteria, to determine efficiencies and to model backgrounds.

Multiple-hit events recorded during the two-week calibration campaign with a ^{60}Co source provided a large sample of Compton scattering events, in which a γ-ray from the ^{60}Co source scatters from an electron in one crystal and is detected in another crystal. The BDTs

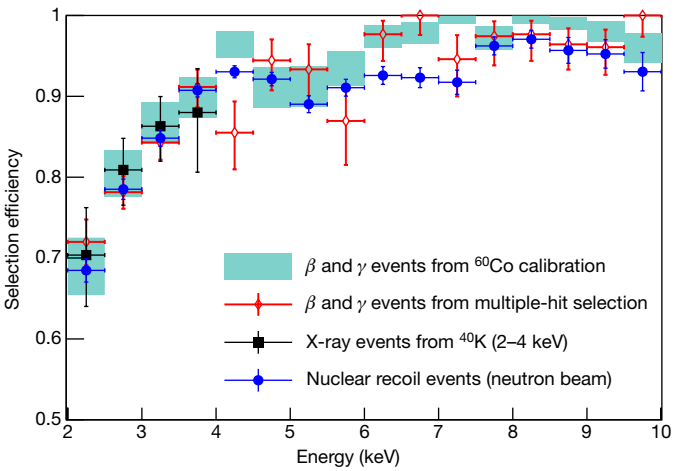

Fig. 1 | Efficiency of event selection. We use various methods to evaluate the efficiency of event selection. The statistical error bands (68% confidence interval) of the event-selection efficiencies determined from the ^{60}Co calibration data are shown as teal shaded regions and are compared with the efficiencies determined from multiple-hit events (red diamonds), internal ^{40}K coincidence events (black squares) and the nuclear-recoil calibration data (blue circles) for one of the crystals. Horizontal error bars depict the bin width of the data. Vertical error bars are 68% confidence intervals.

*A list of participants and their affiliations appears at the end of the paper.

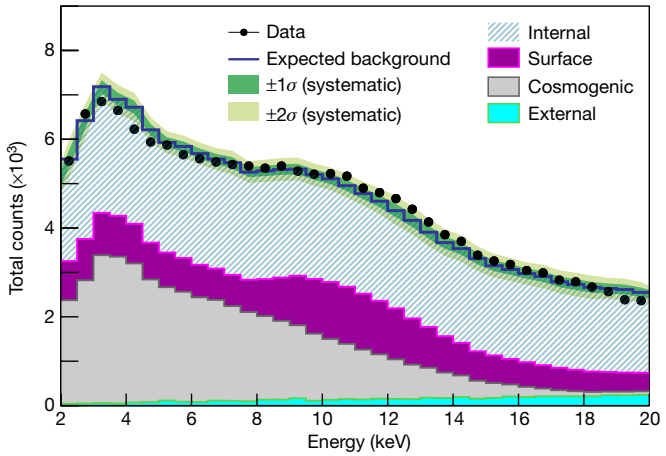

Fig. 2 | Measured and simulated energy spectra. The summed energy spectrum for the six crystals (black filled circles, with error bars (smaller than the symbol size) indicating the 68% confidence interval) and the expected background (blue line) are compared. Contributions to the background from internal radionuclide contaminations (primarily ^{210}Pb and ^{40}K), ^{210}Pb on the surfaces of the crystals and of nearby materials, cosmogenic activation (mostly ^{109}Cd and ^{3}H) and external contaminants (mostly ^{238}U and ^{232}Th) are indicated. The dark green (light green) band is the 68% (95%) confidence interval for the background model. The counts are shown in bins of 0.5 keV.

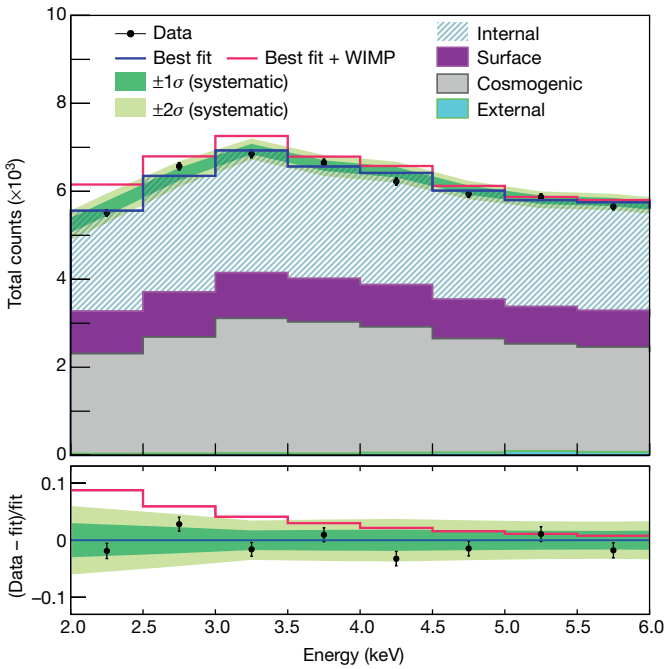

Fig. 3 | Fit results for a WIMP mass of 10 GeV c^{-2}. The data points (black filled circles, with error bars indicating the 68% confidence interval) show the summed energy spectra from the six crystals and the solid blue line shows the result for the fit assuming a WIMP mass of 10 GeV c^{-2}. The expected signal excess above the background for a WIMP mass of 10 GeV c^{-2} and a spin-independent WIMP–nucleon cross-section of 2.35×10^{-40} cm^2 is shown as a solid red line. Coloured regions are as in Fig. 2. The lower panel shows the residuals between the data and the best fit, normalized by the best fit (black filled circles). The bands of systematic uncertainty (dark and light green) and the expected DAMA/LIBRA-phase1 signal spectrum (red) are similarly shown.

are trained for each detector using the multiple-hit events from the ^{60}Co calibration data—weighted to match the energy spectrum of the expected background—and physics data for the signals and the PMT-induced noise (see Methods). The efficiencies of the selection requirements are initially measured with the multiple-hit events from the ^{60}Co source (Fig. 1).

Multiple-hit events from ^{40}K decay are produced when a 3-keV X-ray registers in one crystal and its accompanying 1,460-keV γ-ray registers in another[17]. These events occur throughout the data exposure time and provide independent, real-time energy calibrations and efficiency measurements in the region of interest for the WIMP search (2–6 keV). The efficiencies measured with the multiple-hit events that occur during the dark-matter-search exposure, including tagged 3-keV X-rays from ^{40}K, are in agreement with the efficiencies measured using the ^{60}Co data. A specialized apparatus that has a monoenergetic 2.42-MeV neutron beam is used to measure the selection efficiencies of nuclear recoil events. This measurement was performed with a small test crystal that was cut from the same ingot as one of the crystals used for the COSINE-100 experiment. The efficiencies determined from the different methods are mutually consistent within a 5% level of uncertainty (Fig. 1). The efficiency uncertainties are included as a systematic error.

The remaining dark-matter-search data originate predominantly from environmental γ and β radiation produced from the crystals themselves or from the nearby surrounding materials. Sources include radioactive contaminants inside the crystals or on their surfaces, external detector components and cosmogenic activation[19]. The background spectrum for each individual crystal is modelled using simulations based on the Geant4 toolkit[27]. Multiple-hit events with measured energies between 2 keV and 2,000 keV and single-hit events with measured energies between 6 keV and 2,000 keV are used in the modelling, as described in detail elsewhere[19] (see also Methods). Single-hit events with energies below 6 keV are excluded to avoid a bias against dark-matter signal events. In Fig. 2 we show the summed single-hit event spectrum between 2 keV and 20 keV for the six crystals compared with the simulated contributions from various sources. The data in the 2–6-keV region of interest are within the error bands of the background model.

Several sources of systematic uncertainty were identified and included in the analysis. The largest uncertainties are those associated with the efficiency, which include statistical errors in the efficiency determination with the ^{60}Co calibration and systematic errors derived from the independent cross-checks. Uncertainties in the energy resolution and nonlinear responses of the sodium iodide crystals[28] affect the shapes of the background and signal spectra. These uncertainties are studied using tagged 3-keV X-rays from internal ^{40}K and 59.5-keV γ-rays from an external ^{241}Am source. We also account for different models for ^{210}Pb decays[19] and variations in the levels of external uranium and thorium decay-chain contaminants, as well as the effects of event-rate variations and possible distortions in the shapes of the background model components (Methods).

We used the simulated data to determine the contributions of dark-matter-induced nuclear recoils to the measured energy spectra. Samples of WIMP–sodium and WIMP–iodine spin-independent scattering events were generated for 18 different WIMP masses, ranging from 5 GeV c^{-2} to 10,000 GeV c^{-2}, using the standard WIMP halo model with the same parameters that were used for the WIMP interpretation of the DAMA/LIBRA-phase1 signal[10]. These events were then processed through the detector simulation and the output events were subjected to the same selection criteria that were applied to the data.

To search for evidence of dark-matter-induced events, we performed binned maximum-likelihood fits to the measured single-hit energy spectra between 2 keV and 20 keV for each of the 18 WIMP masses. We used the Bayesian analysis toolkit[29] with probability density functions based on the shapes of the simulated WIMP signal spectra and the various components of the background model. Uniform priors were used for the signals and Gaussian priors were used for the background, with means and uncertainties for each background component set at the values determined from the model fitted to the data[19]. The systematic uncertainties are included in the fit as nuisance parameters with Gaussian priors. To be conservative in the assignment of systematic uncertainties, we consider the maximum allowed distortions of the shapes of the

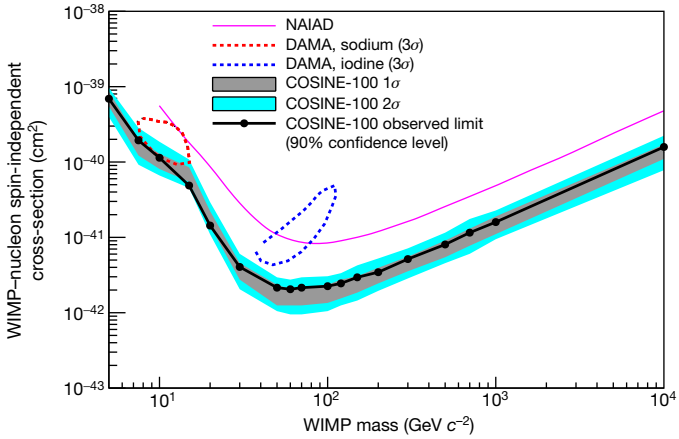

Fig. 4 | Exclusion limits on the WIMP–nucleon spin-independent cross-section. The 90% confidence level exclusion limits on the WIMP–nucleon spin-independent cross-section determined from the data from the first 59.5 days of the COSINE-100 experiment (filled circles and black solid line; total exposure of 6,303.9 kg d) are shown together with their 68% (grey shading) and 95% (blue shading) probability bands assuming the background-only hypothesis. Our exclusion limits are compared with 3σ allowed regions of the WIMP mass and the cross-section associated with the DAMA/LIBRA-phase1 signal for the WIMP–sodium (red dotted contour) and the WIMP–iodine (blue dotted contour) scattering hypothesis[10]. The limit from NAIAD[30]—the only other sodium-iodide-based experiment to set a competitive limit—is shown in purple.

probability density functions within their uncertainties. We also consider the possibility of correlated rate and shape uncertainties and the uncorrelated bin-by-bin statistical uncertainties (Methods). To calculate the expected 90% confidence level upper limits on WIMP–nucleon scattering cross-sections, we performed 1,000 simulated experiments with the expected backgrounds and no dark-matter signal.

Data were fitted to each of the 18 WIMP masses. An example of a maximum-likelihood fit with a 10 GeV c^{-2} WIMP signal is presented in Fig. 3 (see also Extended Data Fig. 5). The summed event spectrum for the six crystals is shown together with the best-fit result. For comparison, the expected signal for a 10 GeV c^{-2} WIMP with a spin-independent cross-section of 2.35×10^{-40} cm^2—the central value of the DAMA/LIBRA-phase1 signal interpreted as a WIMP–sodium interaction—is overlaid in red. No excess of events that could be attributed to standard-halo WIMP interactions are found for the 18 WIMP masses considered. The posterior probabilities of the existence of a WIMP-induced signal are consistent with zero in all cases; we determined 90% confidence level limits. In Fig. 4 we show the 3σ contours of the allowed WIMP mass and the cross-sections that are associated with the DAMA/LIBRA-phase1 signal[10], together with the 90% confidence level upper limits from the COSINE-100 data.

Despite strong evidence for its existence, the identity of dark matter remains a mystery. COSINE-100 continues to collect data, and several years of data will be necessary to fully confirm or refute DAMA's results. However, the first 59.5 days of background data show that the annual modulation in the signal observed by DAMA is inconsistent with spin-independent interactions between WIMPs and sodium or iodine in the context of the standard halo model.

Online content

Any Methods, including any statements of data availability and Nature Research reporting summaries, along with any additional references and Source Data files, are available in the online version of the paper at https://doi.org/10.1038/s41586-018-0739-1.

Received: 27 April 2018; Accepted: 13 September 2018;
Published online 5 December 2018.

1. Clowe, D. et al. A direct empirical proof of the existence of dark matter. *Astrophys. J.* **648**, L109–L113 (2006).
2. Ade, P. A. R. et al. Planck 2015 results. XIII. Cosmological parameters. *Astron. Astrophys.* **594**, A13 (2016).
3. Baer, H., Choi, K.-Y., Kim, J. E. & Roszkowski, L. Dark matter production in the early Universe: beyond the thermal WIMP paradigm. *Phys. Rep.* **555**, 1–60 (2015).
4. Lee, B. W. & Weinberg, S. Cosmological lower bound on heavy-neutrino masses. *Phys. Rev. Lett.* **39**, 165–168 (1977).
5. Goodman, M. W. & Witten, E. Detectability of certain dark matter candidates. *Phys. Rev. D* **31**, 3059–3063 (1985).
6. Battaglieri, M. et al. US cosmic visions: new ideas in dark matter 2017: community report. Preprint at https://arxiv.org/abs/1707.04591 (2017).
7. Bernabei, R. et al. Searching for WIMPs by the annual modulation signature. *Phys. Lett. B* **424**, 195–201 (1998).
8. Bernabei, R. et al. Final model independent result of DAMA/LIBRA-phase1. *Eur. Phys. J. C* **73**, 2648 (2013).
9. Bernabei, R. et al. First model independent results from DAMA/LIBRA-phase2. Preprint at https://arxiv.org/abs/1805.10486 (2018).
10. Savage, C., Gelmini, G., Gondolo, P. & Freese, K. Compatibility of DAMA/LIBRA dark matter detection with other searches. *J. Cosmol. Astropart. Phys.* **4**, 10 (2009).
11. Baum, S., Freese, K. & Kelso, C. Dark matter implications of DAMA/LIBRA-phase2 results. Preprint at https://arxiv.org/abs/1804.01231 (2018).
12. Kang, S., Scopel, S., Tomar, G. & Yoon, J.-H. DAMA/LIBRA-phase2 in WIMP effective models. *J. Cosmol. Astropart. Phys.* **7**, 16 (2018).
13. Barbosa de Souza, E. et al. First search for a dark matter annual modulation signal with NaI(Tl) in the Southern Hemisphere by DM-Ice17. *Phys. Rev. D* **95**, 032006 (2017).
14. Amaré, J. et al. Status of the ANAIS dark matter project at the Canfranc Underground Laboratory. *J. Phys. Conf. Ser.* **718**, 042052 (2016).
15. Fushimi, K. et al. Dark matter search project PICO-LON. *J. Phys. Conf. Ser.* **718**, 042022 (2016).
16. Xu, J., Calaprice, F., Froborg, F., Shields, E. & Suerfu, B. SABRE – a test of DAMA with high-purity NaI(Tl) crystals. *AIP Conf. Proc.* **1672**, 040001 (2015).
17. Adhikari, P. et al. Understanding internal backgrounds in NaI(Tl) crystals toward a 200 kg array for the KIMS-NaI experiment. *Eur. Phys. J. C* **76**, 185 (2016).
18. Adhikari, G. et al. Initial performance of the COSINE-100 experiment. *Eur. Phys. J. C* **78**, 107 (2018).
19. Adhikari, P. et al. Background model for the NaI(Tl) crystals in COSINE-100. *Eur. Phys. J. C* **78**, 490 (2018).
20. Tanabashi, M. et al. The review of particle physics. *Phys. Rev. D* **98**, 030001 (2018).
21. Drukier, A. K., Freese, K. & Spergel, D. N. Detecting cold dark-matter candidates. *Phys. Rev. D* **33**, 3495–3508 (1986).
22. Freese, K., Frieman, J. A. & Gould, A. Signal modulation in cold dark matter detection. *Phys. Rev. D* **37**, 3388–3405 (1988).
23. Lewin, J. & Smith, P. Review of mathematics, numerical factors, and corrections for dark matter experiments based on elastic nuclear recoil. *Astropart. Phys.* **6**, 87–112 (1996).
24. Park, J. S. et al. Performance of a prototype active veto system using liquid scintillator for a dark matter search experiment. *Nucl. Instrum. Methods A* **851**, 103–107 (2017).
25. Prihtiadi, H. et al. Muon detector for the COSINE-100 experiment. *J. Instrum.* **13**, T02007 (2018).
26. Friedman, J. H. Greedy function approximation: a gradient boosting machine. *Ann. Stat.* **29**, 1189–1232 (2001).
27. Agostinelli, S. et al. GEANT4: a simulation toolkit. *Nucl. Instrum. Methods A* **506**, 250–303 (2003).
28. Swiderski, L. Response of doped alkali iodides measured with gamma-ray absorption and Compton electrons. *Nucl. Instrum. Methods A* **705**, 42–46 (2013).
29. Caldwell, A., Kollár, D. & Kröninger, K. BAT – the Bayesian analysis toolkit. *Comput. Phys. Commun.* **180**, 2197–2209 (2009).
30. Alner, G. J. et al. Limits on WIMP cross-sections from the NAIAD experiment at the Boulby Underground Laboratory. *Phys. Lett. B* **616**, 17–24 (2005).

Acknowledgements We thank the Korea Hydro and Nuclear Power (KHNP) Company for providing underground laboratory space at Yangyang. This work is supported by: the Institute for Basic Science (IBS) under project code IBS-R016-A1 and NRF-2016R1A2B3008343, South Korea; UIUC campus research board, the Alfred P. Sloan Foundation Fellowship, NSF grant numbers PHY-1151795, PHY-1457995, DGE-1122492 and DGE-1256259, WIPAC, the Wisconsin Alumni Research Foundation, Yale University and DOE/NNSA grant number DE-FC52-08NA28752, USA; STFC grants ST/N000277/1 and ST/K001337/1, UK; and CNPq and grant number 2017/02952-0 FAPESP, Brazil.

Reviewer information *Nature* thanks B. Sadoulet and the other anonymous reviewer(s) for their contribution to the peer review of this work.

Author contributions Y.K., H.S.L., R.H.M. and N.J.C.S. conceived the COSINE-100 experiment. Its design and installation were led by K.P. and C.H.H. and carried out by all members of the collaboration. Operation and maintenance were organized by C.H.H. with support from on-site crews, W.G.K., B.K. and S.H.Y. Jaison Lee, J.P., J.H.J., G.A., P.A., H. Prihtiadi, C.H.H., W.G.T., E.B.d.S., H.S.L. and K.K. contributed to data acquisition, production and verification. H.J., Hyeonseo Park and K.K. provided nuclear recoil data. P.A., G.A., J.P., K.K., H. Prihtiadi, N.Y.K. and C.H.H. performed the source calibrations. Hyounggyu Kim, N.Y.K., C.H.H. and H.S.L. developed the slow

control framework. J.H.J. and W.G.T. developed the data monitoring package. N.Y.K., Jooyoung Lee and Y.J.K. provided the radiopurity of the detector materials. G.A., J.P. and N.Y.K. produced the liquid scintillator. Background simulations were performed by F.M., E.J., P.A., W.G.T. and E.B.d.S. C.H.H. and P.A. analysed the observational and simulated data. The manuscript and plots were produced by C.H.H. and H.S.L., and edited by R.H.M., S.L.O., N.J.C.S. and the other members of the collaboration. All authors participated in online data-monitoring shifts and approved the manuscript. Authors are listed alphabetically by their last names.

Competing interests The authors declare no competing interests.

Additional information
Extended data is available for this paper at https://doi.org/10.1038/s41586-018-0739-1.
Supplementary information is available for this paper at https://doi.org/10.1038/s41586-018-0739-1.
Reprints and permissions information is available at http://www.nature.com/reprints.
Correspondence and requests for materials should be addressed to C.H.H. and H.S.L.
Publisher's note: Springer Nature remains neutral with regard to jurisdictional claims in published maps and institutional affiliations.

The COSINE-100 Collaboration
Govinda Adhikari[1], Pushparaj Adhikari[1], Estella Barbosa de Souza[2], Nelson Carlin[3], Seonho Choi[4], Mitra Djamal[5], Anthony C. Ezeribe[6], Chang Hyon Ha[7]*, Insik Hahn[8], Antonia J. F. Hubbard[2,16], Eunju Jeon[7], Jay Hyun Jo[2], Hanwool Joo[4], Woon Gu Kang[7], Woosik Kang[9], Matthew Kauer[10], Bonghee Kim[7], Hongjoo Kim[11], Hyounggyu Kim[7], Kyungwon Kim[7], Nam Young Kim[7], Sun Kee Kim[4], Yeongduk Kim[1,7], Yong-Hamb Kim[7,12], Young Ju Ko[7], Vitaly A. Kudryavtsev[6], Hyun Su Lee[7]*, Jaison Lee[7], Jooyoung Lee[11], Moo Hyun Lee[7], Douglas S. Leonard[7], Warren A. Lynch[6], Reina H. Maruyama[2], Frederic Mouton[6], Stephen L. Olsen[7], Byungju Park[13], Hyang Kyu Park[14], Hyeonseo Park[12], Jungsic Park[7,17], Kangsoon Park[7], Walter C. Pettus[2,18], Hafizh Prihtiadi[5], Sejin Ra[7], Carsten Rott[9], Andrew Scarff[6,19], Keon Ah Shin[7], Neil J. C. Spooner[6], William G. Thompson[2], Liang Yang[15] & Seok Hyun Yong[7]

[1]Department of Physics, Sejong University, Seoul, South Korea. [2]Department of Physics, Yale University, New Haven, CT, USA. [3]Physics Institute, University of São Paulo, São Paulo, Brazil. [4]Department of Physics and Astronomy, Seoul National University, Seoul, South Korea. [5]Department of Physics, Bandung Institute of Technology, Bandung, Indonesia. [6]Department of Physics and Astronomy, University of Sheffield, Sheffield, UK. [7]Center for Underground Physics, Institute for Basic Science (IBS), Daejeon, South Korea. [8]Department of Science Education, Ewha Womans University, Seoul, South Korea. [9]Department of Physics, Sungkyunkwan University, Suwon, South Korea. [10]Department of Physics and Wisconsin IceCube Particle Astrophysics Center, University of Wisconsin-Madison, Madison, WI, USA. [11]Department of Physics, Kyungpook National University, Daegu, South Korea. [12]Korea Research Institute of Standards and Science, Daejeon, South Korea. [13]IBS School, University of Science and Technology (UST), Daejeon, South Korea. [14]Department of Accelerator Science, Korea University, Sejong, South Korea. [15]Department of Physics, University of Illinois at Urbana-Champaign, Urbana, IL, USA. [16]Present address: Department of Physics and Astronomy, Northwestern University, Evanston, IL, USA. [17]Present address: High Energy Accelerator Research Organization (KEK), Tsukuba, Japan. [18]Present address: Center for Experimental Nuclear Physics and Astrophysics, Department of Physics, University of Washington, Seattle, WA, USA. [19]Present address: Department of Physics and Astronomy, University of British Columbia, Vancouver, British Columbia, Canada. *e-mail: changhyon.ha@gmail.com; hyunsulee@ibs.re.kr

METHODS

The COSINE-100 experiment is located 700 m below the ground at the Yangyang Underground Laboratory in eastern South Korea. A cut-out view of the detector is shown in Extended Data Fig. 1. It consists of an array of eight sodium iodide 'NaI(Tl)' scintillating crystals (total mass of 106 kg) immersed in 2,200 l of liquid scintillator contained in an acrylic box that is surrounded by copper and lead shielding. Plastic scintillators surround the entire apparatus to detect cosmic-ray muons that penetrate the apparatus. External radiation is attenuated by the lead, copper and liquid scintillator shields. Signals from the liquid scintillator and muon detectors are used to identify background events that are induced by radiation sources in or near the crystals and by cosmic-ray muons. More details about the experimental site, including the fluxes of cosmic-ray muons and neutrons, and the data acquisition system can be found elsewhere[18,25,31].

Event selection. Pulse shapes from the detector are recorded when both PMTs on a crystal record signals that correspond to at least one single photoelectron within 200 ns. In the offline analysis, events are rejected if they occur within 30 ms of a signal from any of the surrounding muon detectors or if there is a signal in the liquid scintillator within 4 μs. Events with and without accompanying hit crystals in an 8-μs time window are classified as multiple-hit and single-hit events, respectively. Events are further classified according to their energy: 2–70 keV is low energy and 70–2,000 keV is high energy.

Extended Data Fig. 2a shows an averaged waveform for radiation-induced scintillation light signals in the NaI(Tl) crystal detectors, where the characteristic 250-ns NaI(Tl) scintillation light decay time is evident. By contrast, PMT noise pulses, which are considerably more frequent, decay faster, with decay times ranging between 20 ns and 50 ns (Extended Data Fig. 2b). Some detectors intermittently produce events that have slow rise and decay times (Extended Data Fig. 2c); these are attributed to PMT discharges.

We use BDTs to separate signal events from noise events. The fast PMT noise-induced events are efficiently removed by a BDT that is based on the amplitude-weighted average time of a signal, the ratios of the leading-edge and trailing-edge charge sums relative to total charge, and the balance of deposited energies between the two PMTs. This BDT is trained with a sample of signal-rich, energy-weighted, multiple-hit events from the ^{60}Co calibration and single-hit events from the WIMP-search data; the latter are mostly triggered by PMT noise. A second BDT (BDTA) that includes weighted higher-order time moments is effective at eliminating discharge events. Extended Data Fig. 3 shows two-dimensional scatter plots of the BDT and BDTA outputs for two separate crystals, one with and the other without PMT discharge signals. Events that are above and to the right of the dashed red lines in the figure are retained.

Background modelling. The primary background components of the energy spectra of the crystals are from internal ^{238}U, ^{232}Th, ^{40}K and ^{210}Pb contaminations in the bulk material of the crystal, plus additional ^{210}Pb on the surfaces of the crystal and its reflective wrapping foil, caused by exposure to atmospheric radon during the encapsulation of the crystals[19]. In addition, we considered background from external sources such as ^{238}U, ^{232}Th and ^{40}K contaminations in the PMTs, the liquid scintillator and the bulk material of the surrounding shields. The modelling of these contributions used starting values based on radioassay results from an underground, high-purity Ge detector[32]. The modelling of contributions from cosmogenic activity in the crystals was guided by measured surface production rates in NaI(Tl)[33] and the above- and below-ground histories of each individual crystal.

In 10.7% of ^{40}K decays, a roughly 3-keV K-shell X-ray (or Auger electron) is produced in coincidence with a 1,460-keV γ-ray. Because this results in a peaking background in the WIMP search region of interest, it is of particular concern. However, in the COSINE-100 detector, about 80% of these 3-keV X-rays are tagged by the detection of its accompanying 1,460-keV γ-ray in one of the other crystals or in the liquid scintillator and so can be vetoed. The measured rate for these tagged events is used to establish the contribution of untagged 3-keV ^{40}K-induced events to the background in the region of interest for the single-hit spectrum in each crystal.

Extended Data Fig. 4 shows the results of the model fits to the data for the four categories of events (single-hit and multiple-hit events in low and high energy), with 1σ and 2σ uncertainty bands indicated in green and yellow, respectively[19]. All four distributions were fitted simultaneously. To avoid biasing the WIMP search, the 2–6-keV region of the low-energy, single-hit spectrum (Extended Data Fig. 4a) is not included in the fitting. The fitted model indicates that the main contributions in the 2–6-keV region of interest are from internal ^{40}K and ^{210}Pb, and cosmogenic ^{109}Cd and ^{3}H. The ^{109}Cd contribution was confirmed independently by a time-dependent analysis.

Systematic uncertainties. The results of the analysis are limited by the systematic uncertainties. Errors in the selection efficiency, energy resolution, energy scale and background modelling technique translate into uncertainties in the shapes of the probability density functions of the signal and background components that are used in the likelihood fit, and thus affect the results. These quantities are allowed to vary within their errors in the likelihood as nuisance parameters. Of these, the systematic errors associated with the efficiencies have the largest effects on the results. Uncertainties in the efficiencies are determined by the statistical errors from the data from the efficiency measurements for the multiple-hit ^{60}Co source, and their stability is verified by independent datasets (Fig. 1). The efficiency systematic that maximally covers the statistical errors in the region of interest mimics the shape of a WIMP signal.

For most of the energy range, the resolutions and scales are well measured with internal radioactive peaks and external calibrations. However, because external source measurements are impractical for energies below 10 keV, the resolution and scale values for these energies are determined with the samples of tagged 3-keV X-rays from the internal ^{40}K contamination. For these, statistical errors dominate and are taken as the systematic spread from these quantities. We used changes that occur in the background model when the simulation is done with different locations of the U/Th contamination in the PMTs, and alternative Geant4 methods for X-ray production of ^{210}Pb, as the systematic error from this source. The inclusion of the total systematic uncertainties degrades the sensitivity by a factor of 2.3.

WIMP extraction Bayesian fit. A Bayesian analysis with a likelihood formulated in equation (1) was performed and this fitter, which is more computationally demanding than the background modelling fits, was run with the WIMP-search data (low-energy single-hit spectrum) between 2 keV and 20 keV. The function that is maximized has the form

$$\mathcal{L}=\prod_{i}^{N_{\mathrm{ch}}}\prod_{j}^{N_{\mathrm{bin}}}\frac{\mu_{ij}^{n_{ij}}}{n_{ij}!}\exp(-\mu_{ij})\prod_{k}^{N_{\mathrm{bkg}}}\exp\left[-\frac{(x_k-\alpha_k)^2}{2\sigma_k^2}\right]\prod_{l}^{N_{\mathrm{syst}}}\exp\left(-\frac{x_l^2}{2\sigma_l^2}\right) \quad (1)$$

where N_{ch} is the number of crystals, N_{bin} is the number of bins in each histogram, N_{bkg} is the number of background components, N_{syst} is the number of systematic nuisance parameters, n_{ij} is the number of observed counts and μ_{ij} is the total model expectation by summing all N_{bkg} background components and a WIMP signal component after apply a shape change due to N_{syst} systematic effects. In the first product of Gaussians, x_k is the value of the kth background component, α_k is the mean value and σ_k is its 68% error. The second product of Gaussians x_l is the lth systematic parameter and σ_l is its error.

To avoid biasing the WIMP search, the fitter was developed and tested with simulated event samples. All eight crystals are fitted simultaneously with a common WIMP-signal model for each assumed WIMP mass and with fits performed for 18 different WIMP masses between 5 GeV c^{-2} and 10,000 GeV c^{-2}. The shapes of the energy spectra of the WIMP signal are determined from simulations based on the standard WIMP halo model with parameters taken from ref. [10]. To relate the simulated WIMP signals, which are caused by nuclear recoils, to our energy scale, which is calibrated with electron recoils, we use the same NaI(Tl) quenching factors that were used in interpretations of the DAMA/LIBRA-phase1 signal, $Q_{\mathrm{Na}}=0.3$ and $Q_{\mathrm{I}}=0.09$ (quenching factors are the ratio of scintillation-light energy determinations for nuclear and electron recoils of the same energy).

We use Gaussian priors for the normalizations of the background components and the systematic nuisance parameters for efficiencies, energy resolutions and energy scales. The initial values for the background-component normalizations are taken from the fits described above that do not use the single-hit events in the 2–6-keV region of interest. The final fit values for all nuisance parameters are within $\pm1\sigma$ of their initial values.

Code availability. All data related to the analysis are in the ROOT (https://root.cern.ch) format. Analysis toolkits such as ROOT, including BDT and BAT (https://bat.mpp.mpg.de), are available online. Our custom codes are available from the corresponding authors on reasonable request.

Data availability

The data that support the findings of this study are available from the corresponding authors on reasonable request. Source Data for Figs. 1–4 are provided with the online version of the paper.

31. Adhikari, G. et al. The COSINE-100 data acquisition system. *J. Instrum.* **13**, P09006 (2018).
32. Sala, E. et al. Development of an underground low background instrument for high sensitivity measurements. *J. Phys. Conf. Ser.* **718**, 062050 (2016).
33. Pettus, W. C. *Cosmogenic Activation in NaI Detectors for Dark Matter Searches*. PhD thesis, Univ. Wisconsin–Madison (2015).

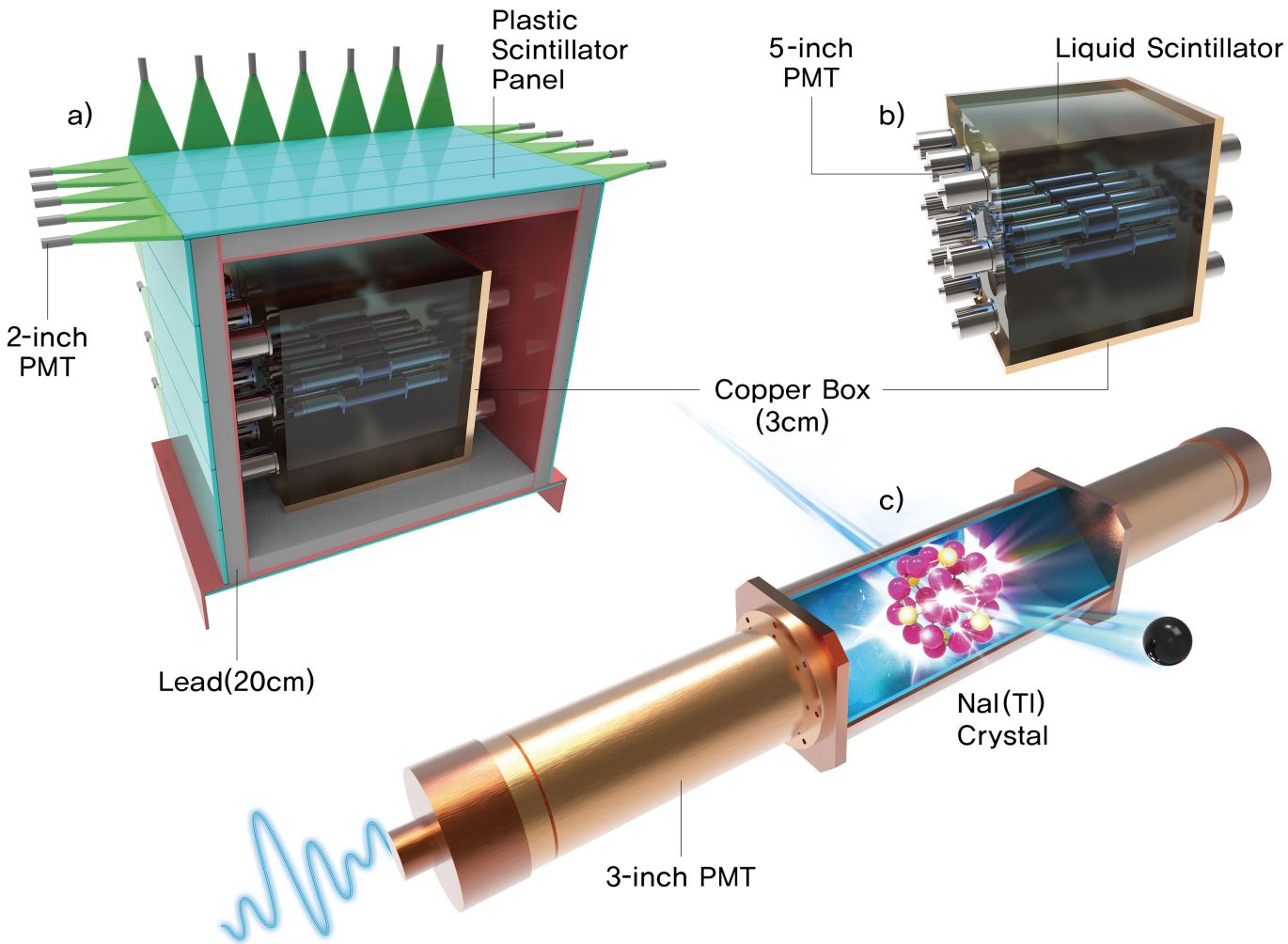

Extended Data Fig. 1 | The COSINE-100 detector. a, The detector is contained within a nested arrangement of shielding components, as indicated by different colours. The main purpose of the shield is to provide 4π coverage against external radiation from various background sources. The shielding components include plastic scintillator panels (blue), a lead brick enclosure (grey) and a copper box (reddish brown). **b**, **c**, The eight encapsulated sodium iodide crystal assemblies (**c**) are located inside the copper box and are immersed in scintillating liquid (**b**). All images are schematic.

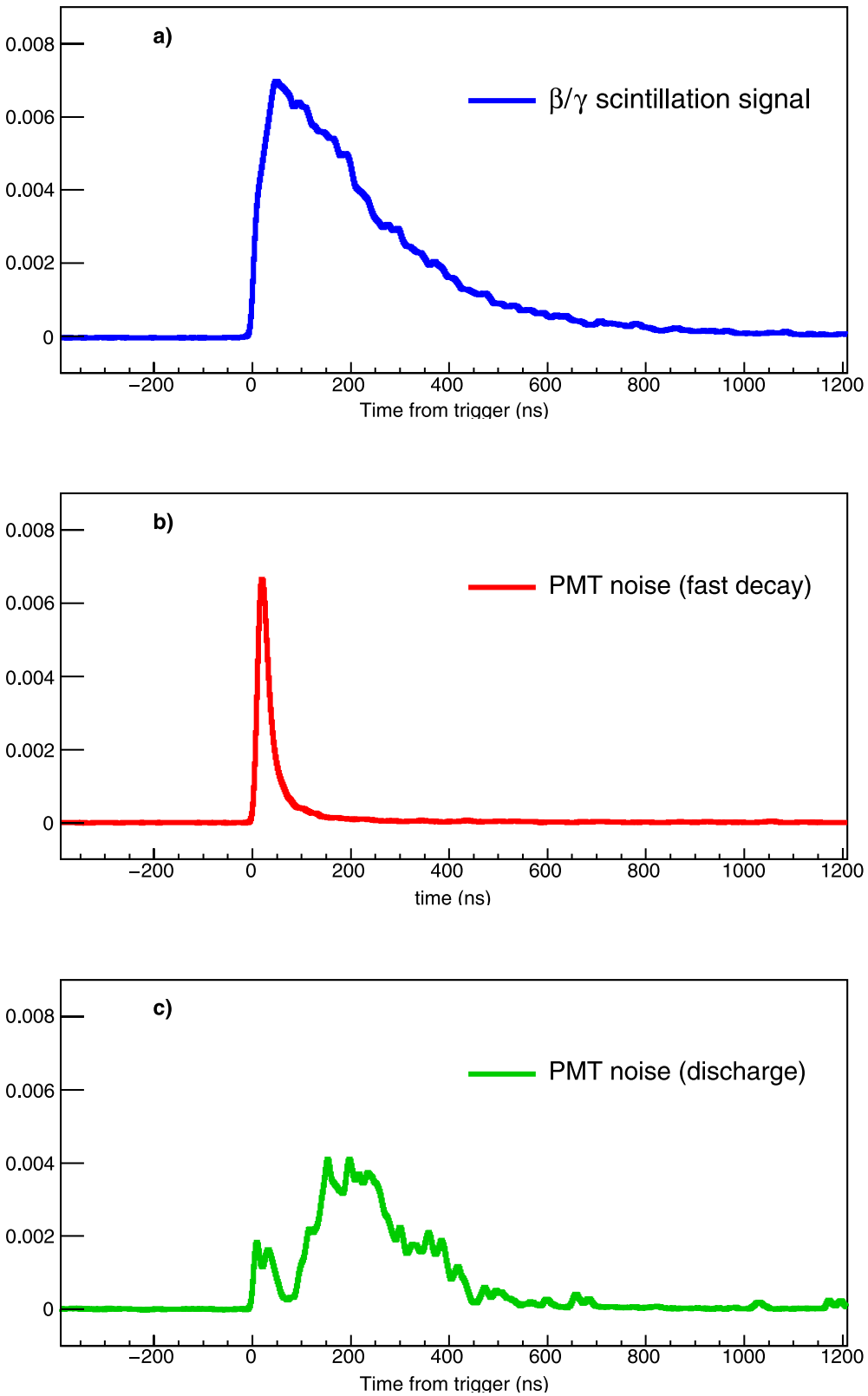

Extended Data Fig. 2 | Typical waveforms from the COSINE-100 PMTs for 2–6-keV signals. a, The β and γ scintillation signals have a fast rise and then fall off with a decay time of about 250 ns. The waveform from WIMPs is expected to closely resemble the β and γ waveforms. **b**, **c**, Background waveforms from PMT noise (**b**) and external discharge (**c**).

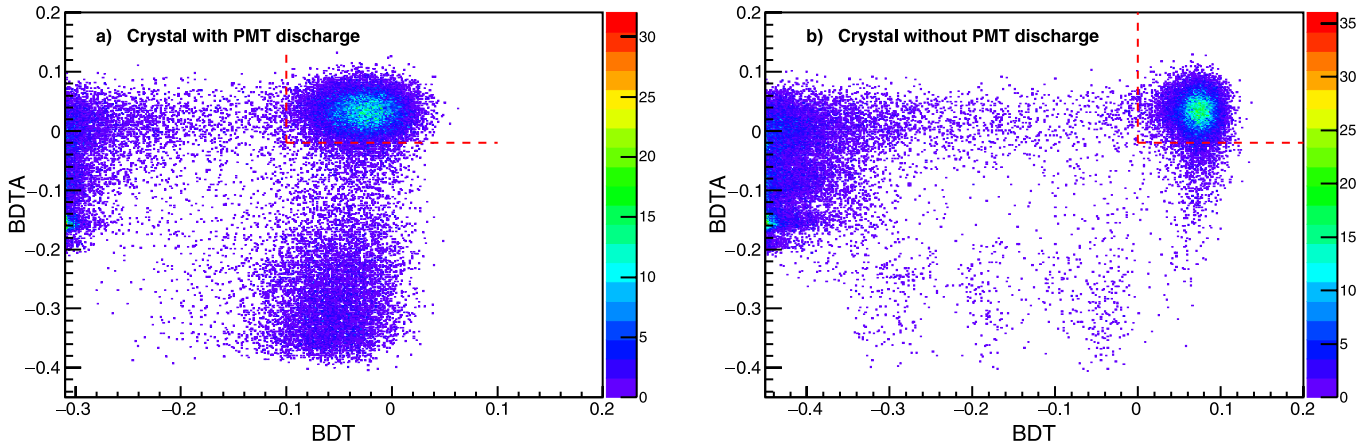

Extended Data Fig. 3 | The BDT output (horizontal) versus the BDTA output (vertical). a, **b**, Events (colour scale) with energies below 10 keV are shown for two separate crystals, with (**a**) and without (**b**) PMT discharge. The events to the right and above the red dotted lines are scintillation events induced by real particle–crystal interactions. PMT noise events are to the left of the vertical dotted lines in both panels; PMT discharge events are below the horizontal dotted line in **a**.

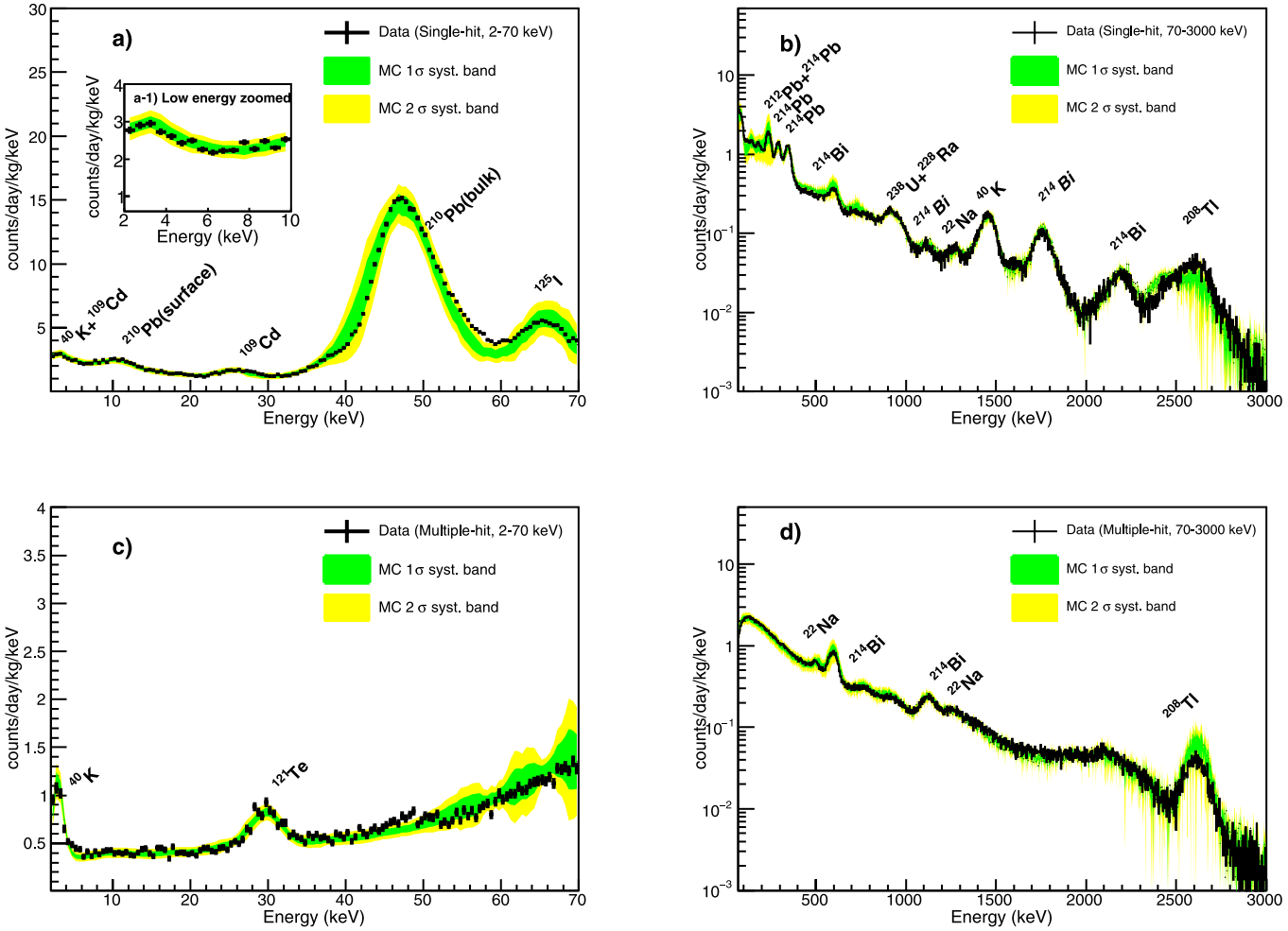

Extended Data Fig. 4 | A comparison between data and simulation. **a**–**d**, Four categories of data are shown: single-hit low-energy (2–70 keV; **a**); single-hit high-energy (70–3,000 keV; **b**); multiple-hit low-energy (2–70 keV; **c**); and multiple-hit high-energy (70–3,000 keV; **d**). The black points (with errors bars indicating the 68% confidence interval) are data. The green (yellow) band shows the $\pm 1\sigma$ ($\pm 2\sigma$) uncertainty range of the model. The peak near 3 keV in the multiple-hit, low-energy spectrum (**c**) is due to the tagged ^{40}K events. The inset in **a** shows a zoomed-in view in the region of interest after efficiency corrections are applied. The major contributors to the radioactive background are labelled.

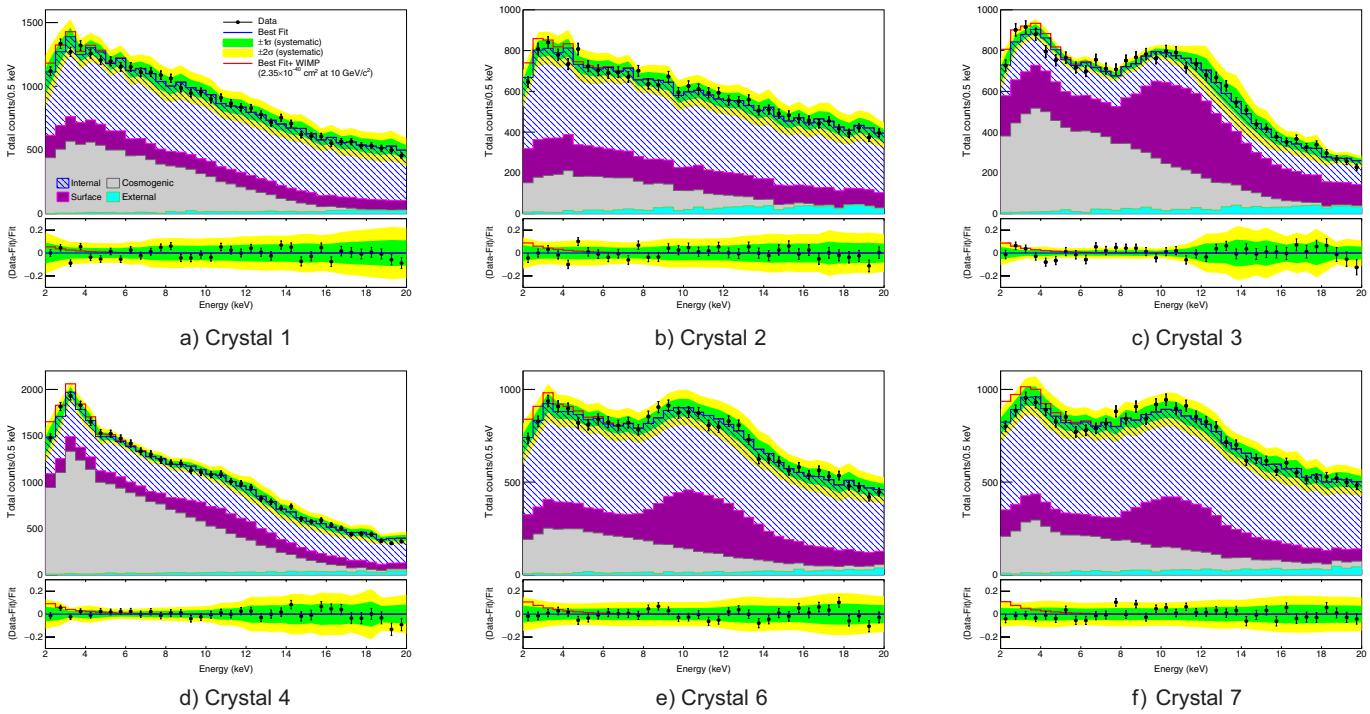

Extended Data Fig. 5 | Crystal-by-crystal fit results. a–f, The points (with errors bars indicating the 68% confidence interval) show the measured energy spectra for each of the six crystals. The fit results are shown as blue histograms, with the $\pm 1\sigma$ ($\pm 2\sigma$) error bands shown in green (yellow). To compare the signal strength of the DAMA sodium region with our data, a 10 GeV c^{-2} WIMP signal at 2.35×10^{-40} cm^2 (the centre of the DAMA sodium region) is indicated for each crystal as a red histogram. The fit residuals, together with the expectations for the 10 GeV c^{-2} WIMP signal are also shown (bottom panels).